Available online at www.sciencedirect.com
SCIENCE DIRECT®
Journal of Molecular Graphics and Modelling 23 (2004) 139–152
Journal of Molecular Graphics and Modelling
www.elsevier.com/locate/JMGM

Molecular basis of the constitutive activity and STI571 resistance of Asp816Val mutant KIT receptor tyrosine kinase

Rowan Foster [a], Renate Griffith [b,*], Petranel Ferrao [a], Leonie Ashman [a]

[a] School of Biomedical Sciences, Faculty of Health, University of Newcastle, Callaghan NSW 2308, Australia
[b] School of Environmental and Life Sciences, Faculty of Science and IT, University of Newcastle, Callaghan NSW 2308, Australia

Received 11 February 2004; received in revised form 27 April 2004; accepted 27 April 2004

Available online 7 June 2004

Abstract

The receptor tyrosine kinase, KIT, displays activating mutations in the kinase domain, which are associated with various cancers. We have used homology modelling based on the crystal structures of the insulin receptor kinase in active and inactive conformations to predict the corresponding structures of the KIT kinase domain. We have prepared four KIT models, one each for the active and inactive conformations of the wild-type and of the Asp816Val mutant proteins. We have also placed ATP into the active conformations and the inhibitor, STI571, into the inactive conformations. All models have been fully energy minimised. The molecular modelling studies described here explain (i) why Asp816Val KIT is constitutively active, (ii) why the nature of the substituting amino acid at residue 816 is relatively unimportant, and (iii) why the Asp816Val substitution confers resistance to the KIT-inhibitory drug STI571. The models will be valuable for predicting other kinase inhibitory drugs that may be active on wild-type and mutant forms of KIT. During the course of this work, a crystal structure of the active conformation of the KIT kinase domain has been published. Our model of the active conformation of the Asp816Val mutant is strikingly similar to this crystal structure, whereas our model of the active conformation of the wild-type kinase domain of KIT differs from the crystal structure in some respects. The reasons for this apparent discrepancy are discussed.

Keywords: Homology modelling; Receptor tyrosine kinase; Constitutive activity; Drug resistance; Active conformation; Inactive conformation; Activating mutation

1. Introduction

c-*KIT*, originally identified as the normal cellular homolog of the v-*kit* oncogene encodes a type 3 receptor tyrosine kinase (RTK) [1,2]. Like other type 3 RTKs, the colony-stimulating factor 1 receptor (CSF-1R), the platelet-derived growth factor receptor (PDGFR) and the FLT-3 RTK, the KIT protein consists of five Ig-like loops in the extracellular domain, a single transmembrane domain, and a cytoplasmic tyrosine kinase domain split by a 77 amino acid insert (reviewed [3]). KIT plays a key role in hemopoiesis, melanogenesis, fertility and gut motility (reviewed, [4]).

Activation of RTKs occurs as a result of ligand-induced dimerisation/oligomerisation resulting in trans-phosphorylation of receptor monomers. The kinase domains exist in at least two conformations characterised largely by the position of the activation loop which, in the inactive conformation, masks the active site [5,6]. Phosphorylation of tyrosines in the activation loop is believed to stabilise the kinase in the active conformation where the loop is moved away from the substrate-binding region. Other phosphorylation events create docking sites for SH2 and PTB domains of downstream signalling molecules, initiating the signalling cascade [7]. The kinase domains of RTKs and other protein kinases are highly conserved in relation to sequence and overall structure [8]. Crystal structures of the kinase domains of several RTKs have been determined [9–11].

KIT is expressed in many forms of cancer, such as acute myeloid leukaemia (AML), systemic mastocytosis, melanoma and gastrointestinal stromal tumours (GIST), in general reflecting its pattern of expression in normal tissues [12]. Two classes of mutation have been reported to lead to constitutive activation. Mutations resulting in deletions, duplications, or substitutions in the intracellular juxtamembrane domain, a known negative regulatory region of KIT and other RTKs [13,14], are primarily associated with

* Correspondence. Tel.: +61 2 4921 6990; fax: +1 61 2 4921 6923.
E-mail address: renate.griffith@newcastle.edu.au (R. Griffith).

1093-3263/$ – see front matter © 2004 Elsevier Inc. All rights reserved.
doi:10.1016/j.jmgm.2004.04.003

GIST. Point mutations leading to substitutions of Asp816 in the kinase domain are found in mastocytosis with underlying myelodysplasia, occasional cases of AML, germ cell tumours and sinonasal lymphoma [12,15–21]. In other cancers, for example breast, small cell lung cancer and neuroblastoma, autocrine or paracrine cycles involving KIT and its ligand appear to be important for tumour growth [22–27]. Thus, KIT is an important target for directed therapy in cancer. Furthermore, the crucial role of KIT in normal mast cell biology indicates potential applications for inhibitors also in cases of mastocytosis without underlying KIT mutations.

Wild-type KIT is inhibited by the ATP-competitive 2-phenylaminopyrimidine derivative, STI571 (also known as Gleevec or Imatinib) with similar IC_{50} to the fusion protein between the product of the breakpoint cluster region and the Abelson tyrosine kinase (BCR/ABL), its target in chronic myeloid leukaemia (CML) [28–30]. Mutant forms of KIT vary greatly in their sensitivity to the drug. Substitutions at position Asp816 in the kinase domain render KIT almost completely resistant to STI571, while mutations affecting the intracellular juxtamembrane region of the receptor leave sensitivity similar or enhanced [31,32]. Thus GISTs, which characteristically have juxtamembrane KIT mutations [18,19,33,34] are good candidates for STI571 therapy, while cases of systemic mastocytosis with mutations affecting amino acid 816 are not [35,36]. STI571 was recently approved for treatment of metastatic and/or unresectable GIST [37]. Experience with STI571 in treatment of BCR/ABL-driven malignancies has indicated that development of resistance due to point mutations in the kinase domain is a serious problem [38,39]. Thus, it might be predicted that tumours with initially sensitive forms of mutant KIT could develop resistance due to subsequent mutation(s) affecting Asp816 or other amino acids in the kinase domain. The sequential acquisition of activating mutations of the two classes, resulting in STI571 resistance, is demonstrated by the HMC-1 cell line [12,31,40].

In this paper we describe the use of molecular modelling approaches based on the known crystal structures of active and inactive conformations of the insulin receptor kinase (IRK) to determine the basis of constitutive activation of Asp816 mutant KIT, and to explain why this mutant form is resistant to inhibition by STI571. The models provide a basis for predicting other kinase inhibitors that may be active on wild-type and kinase mutant forms of KIT.

2. Methodology

2.1. Sequence alignment

The sequence of the kinase domain of KIT was aligned with those of related kinases for which crystal structures are available, using the program CLUSTALW [41]. Aligned sequences were adjusted manually in Swiss-PdbViewer with the CLUSTALW alignment as a guide to accommodate the insert region, which is not conserved between kinases.

2.2. Initial homology models

Three dimensional models of the KIT kinase domain were constructed from the sequence alignments, using SWISS-MODEL version 3.7 [42] based on the crystal structures of inactive and active IRK kinase domains as templates [11,43]. The two IRK structures are referred to here as IRK_a for the active structure (pdb code 1ir3) and IRK_i for the inactive structure (pdb code 1irk). The sequences of IRK_i and IRK_a have, respectively, 41.9 and 37.1% sequence identity with KIT and the two crystal structures are of 2.1 and 1.9 Å resolution, making them good templates. The crystal of IRK_i contains only one protein molecule per unit cell, whereas that of IRK_a contains two. Chain A was used as this contains a more complete set of coordinates.

The insert region of KIT was automatically modelled by SWISS-MODEL using a library of pentapeptides. The homology models for KIT based on the inactive and active templates, were termed Asp816KIT_i and Asp816KIT_a respectively. Models for the corresponding constitutively active mutant (Val816KIT) were also prepared and were called Val816KIT_i and Val816KIT_a.

Energy minimisation was performed using the GROMOS96 force field by SWISS-MODEL (200 steps of Steepest Descents, followed by 500 cycles of Conjugate Gradients with no constraints).

2.3. Refinement of models

The initial models were imported into SYBYL (SYBYL 6.9 Tripos Inc., St Louis, MO, USA). For the models of active conformations, two Mg^{2+} ions were placed into the same positions as those observed in the crystal structure. Every model went through a multi-step refinement process. Atom types were checked (incorrectly assigned ones were changed), hydrogens were added, and partial charges loaded from a library (Kollmann_all). The proprietary Tripos force field was used throughout, without explicit water molecules or implicit solvation models. The models were subjected to constrained energy minimisation, where first all heavy atoms were fixed, then only the backbone, then they were minimised without any constraints, using the Steepest Descents algorithm. Further energy minimisation was carried out by performing Powell Conjugate Gradient optimisation, until the maximum derivative became less than 0.01 kJ/(mol Å).

2.4. Evaluation of refined models

The refined structures were subjected to a series of three tests for internal consistency and reliability. Backbone conformation was evaluated via the Ramachandran plot obtained from PROCHECK [44] analysis. Geometry was investigated

by WHATIF [45]. Secondary structure was predicted using PredictProtein [46].

2.5. ATP and inhibitor docking

A model of ATP was built in SYBYL in the same conformation as the ATP analogue in the IRK_a crystal structure. The kinase inhibitor STI571 was extracted from the ABL crystal (pdb code 1iep) [47]. The two structures were imported into SYBYL as described for the protein models, partial charges were calculated by the Gasteiger method in SYBYL. The ligands were docked into the refined models by hand, using the crystal structures as a guide and the complexes energy-minimised in stages as described above.

2.6. Phosphorylation

Tyr823 was modified to phosphoTyr in all four KIT models, then each model was energy minimised as previously described.

2.7. Comparison of models

Quantitative comparisons on a residue-by-residue basis were performed using ProFlex, which employs a difference distance matrix (DDM) approach [48]. Superimpositions were performed in SYBYL and in SWISS-MODEL. Except where otherwise indicated, the models of active conformations of KIT (Asp816KIT_a and Val816KIT_a) discussed in the following sections are unphosphorylated at Tyr823 and contain ATP docked into them. Energy values after minimisation were compared for the models, despite the fact that force field energies are—strictly speaking—only comparable for identical molecules and complexes. Since the wild-type and mutant models differ in only one residue, it was felt that the energies are an important indication of relative stabilities.

3. Results

3.1. Sequence alignment, template choice and validation

Several kinase domain crystal structures are available as potential templates for modelling KIT. Fig. 1 shows an alignment of KIT, fibroblast growth factor receptor (FGFR) 1 and 2, vascular endothelial growth factor receptor (VEGFR) 2, ABL, and IRK kinase domains produced with CLUSTALW. Several residues, indicated #, are highly conserved in all protein kinases. Asp816 in KIT (boxed in Fig. 1), which is of particular interest here, is conserved in the other RTKs but not in ABL. IRK is the only receptor kinase with sufficient homology to KIT (40%) where structures are available in both active and inactive conformations at high resolution [11,43]. Since direct comparison of structures of the same protein in the active and inactive conformations was of crucial importance to this work, the IRK structures were chosen as templates in preference to the FGFR1 and 2, and VEGFR2 structures. The IRK structure representing an active conformation, referred to as IRK_a here, is complexed with an analogue of ATP, adenylyl imidodiphosphate (AMP-PNP) [11]. The inactive conformation is referred to as IRK_i.

As expected from the moderate degree of sequence identity, the backbone configurations of the KIT models generated by SWISS-MODEL from these alignments and minimized in the SYBYL software environment were very similar to the two IRK templates. The backbone root mean square deviations (RMSDs) of the inactive models from their respective templates were low (0.9 and 1.0 Å) for Asp816KIT_i and Val816KIT_i. The active models had RMSD values of 1.2 and 0.9 Å for models Asp816KIT_a and Val816KIT_a. Secondary structure prediction with PredictProtein matched all the features found in models and templates.

We used the program PROCHECK to validate the templates and models based on stereochemical and geometric considerations. PROCHECK bases its evaluation on an analysis of 118 protein crystal structures of resolution below 2 Å and presents the results as Ramachandran plots of backbone torsion angles (Psi versus Phi, data not shown). From the analysis of the crystal structures, the program has divided the torsion angle space into ‘most favoured regions’, two kinds of ‘allowed regions’ and ‘disallowed regions’ for all amino acids except Pro and Gly and the two end residues of a chain. Homology models are expected to show similar, possibly slightly lower quality than the template crystal structures they are based on, when evaluated with PROCHECK, and a good quality model would be expected to have over 90% of Psi/Phi angles in the most favoured regions. The two templates used here, IRK_i and IRK_a, show somewhat lower quality than expected from their resolution. For the IRK_i template two residues were in the disallowed regions and 89% of residues were found in ‘most favoured regions’. No residues were in the disallowed region and 89% of residues were in ‘most favoured regions’ for the IRK_a template. For our models, five and two residues were in disallowed regions and 76 and 81% of residues were in ‘most favoured regions’ for Asp816KIT_i and Val816KIT_a, respectively. These indicators show that both models are structurally acceptable, especially when taking into account the large insert sequence not present in the templates.

We also evaluated the models in more detail using WHATIF. The results are summarised in Table 1. WHATIF judged forbidden Psi/Phi angles more stringently than PROCHECK, and labelled nine residues as in forbidden areas for the two crystal structures used as templates (IRK_i and IRK_a). The forbidden Psi/Phi combinations in the models still meant that only between 9 and 14% of residues were in forbidden areas, which is acceptable. The models of wild-type KIT show more problems with the geometry of the residues than the Val816 mutant models. In

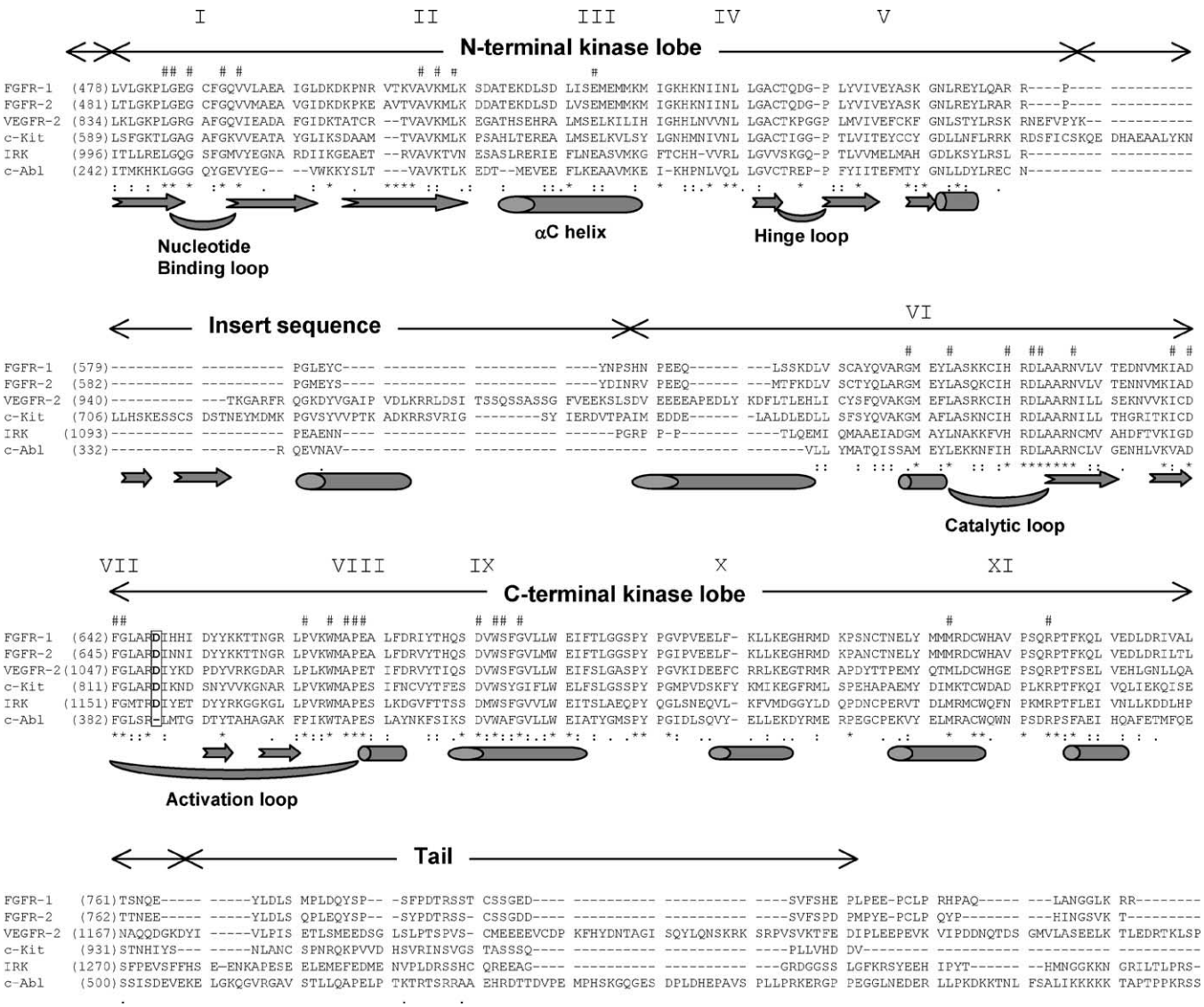

Fig. 1. CLUSTALW sequence alignment of the kinase domains of KIT (p10721), IRK (p06213), FGFR1 (p11362), FGFR2 (p21802), ABL (p00519), and VEGFR2 (p35968). Roman numerals indicate conserved sub-domains in the protein kinase family, as defined by Hank et al. (1988). Residues marked with an # above the sequence are conserved in the protein kinase family. Asp816 is highlighted in bold text and boxed. Below the sequence, (*) indicates identical amino acids, (:) represents highly conserved substitutions, (.) represents conserved substitutions and gaps, marked by (–) are in the sequence to optimise the alignment. Secondary structure elements in KIT are below the sequences: cylinders for helices and arrows for ß-strands.

Table 1
Geometry checks performed on wild-type and Val816 mutant KIT models and on crystal structure templates by WHATIF[a]

Structure	Unusual bond angles[b]	Unusual bond lengths[b]	Forbidden Psi/Phi combinations	Energy after refinement (kcal/mol)
IRK_i	4 (4)	0	9	N/A
Asp816KIT_i	92 (64)[c]	13 (7)[d]	52	−1494
Val816KIT_i	36 (19)	0	35	−1031
IRK_a	2 (2)	0	9	N/A
Asp816KIT_a	83 (47)	18 (8)	27	−507[e]
Val816KIT_a	75 (45)[f]	13 (5)[d]	29	−3726[e]

[a] Crystal structure resolution set to 2 Å in all cases.
[b] Number of residues involved given in brackets.
[c] Includes 11 Pro, 8 His.
[d] Includes only sidechains of His and Trp residues.
[e] Includes ATP docked into models.
[f] Includes 15 Pro, 9 His.

particular, the Asp816KIT_i model showed more violations than the Val816KIT_a model, despite being lower in energy (see Section 2 for a discussion of energy values). We thus decided to analyse the violations in more detail and found that for both the Asp816KIT_i and the Val816KIT_a models, which correspond to the lower energy inactive and active conformation, respectively, the unusual bond lengths only occur in His and Trp sidechains, and the unusual bond angles are concentrated in Pro and His residues (Table 1). We therefore suspect that this is a problem related to the forcefield parameters for these residue types.

3.2. General overview of models

Ribbon traces of the wild-type KIT models (Fig. 2) show the bilobal structure common to all protein kinases, and the secondary structural elements (see also Fig. 1) are designated according to the convention given to cyclic AMP-dependant protein kinase (protein kinase A) [49]. The first 93 residues of the small N-terminal kinase lobe contain a five strand antiparallel β-sheet structure and one helix (αC). Another characteristic and highly conserved feature of receptor tyrosine kinases [50], the Gly-rich ATP binding sequence motif, is located between strands β1 and β2. The larger C-terminal kinase lobe is dominated by seven α-helices. Three short β-strands lie at the 'top' of the C-lobe adjacent to the N-lobe β-sheet forming a small 'nest-like' shape. ATP is bound at the interface of the two lobes and is orientated for phosphoryl transfer by interactions with residues highly conserved among kinases [51].

Important loop regions include the Gly-rich nucleotide binding loop (residues 596–601), the catalytic loop (residues 786–796), and the activation loop (residues 810–839), which also includes the substrate-binding P + 1 loop (residues 829–837). Residues 805–807 preceding the activation loop are termed hinge residues. In KIT the N-lobe and the C-lobe are connected via an insert sequence of 77 amino acids, which is not necessary for kinase activity but is an important

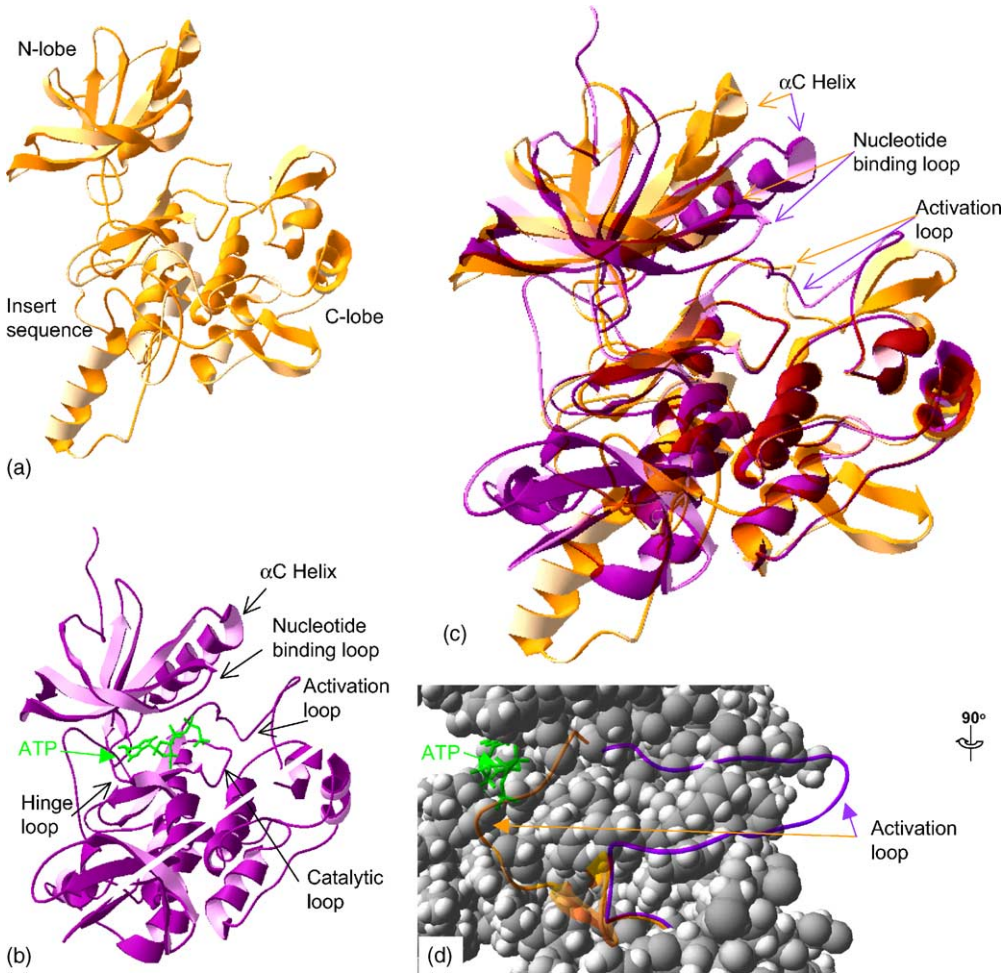

Fig. 2. Ribbon traces for the backbone conformations of KIT models. (a) Asp816KIT_i (orange) (b) Asp816KIT_a (purple) with ATP docked (in green stick); (c) Superimposition of the two models; colours as for (a); (d) Detailed view of the superimposition shown in (c), rotated by 90° out of the plane of the paper. ATP (in green stick) has also been added, as well as all atoms of the models in grey, space filling rendering. For the two different traces of the activation loop, only the backbones are shown for clarity as ribbons (colours as for a).

autophosphorylation and docking site for other proteins including phosphatidylinositol 3-kinase and GRB2 [52,53]. As the IRK template lacks a kinase insert, the structure of this insert was only approximated by SWISS-MODEL, therefore it is not reliable and will not be discussed further. The C-terminal tail of KIT contains a tyrosine known to bind to GRB2/GRB7 [53]. This region is also missing from the IRK crystal structures and thus could not be modelled.

3.3. Structural changes to KIT upon activation

Superimposition of all Cα atoms of models of wild-type KIT (Asp816KIT_i and Asp816KIT_a) resulted in a small RMSD value of 1.3 Å. Similarly, superimposition of all Cα atoms of mutant Val816KIT_i and Val816KIT_a produced an RMSD value of 1.4 Å. However, as can be clearly seen in Fig. 2c and d, large changes can be observed between the inactive and active conformations in specific regions. The superimposition for Figs. 2 and 5 was performed in SWISS-MODEL, using the interactive 'Iterative Magic Fit' option. This option performs a superimposition based on a structural alignment. Very similar results were obtained when performing the superimpositions in SYBYL using the 'Biopolymer fit' feature. The difference distance matrix (DDM) method [48] which measures distances between all pairs of Cα atoms of each structure and then compares the resulting matrices for two (or more) structures was also used to quantitate changes (see Fig. 3). Comparisons between the inactive and active conformations for both the wild type and mutant models revealed three main regions (apart from the insert sequence) of very large movements (greater than 7 Å) in each DDM, which corresponded to the αC helix, the activation loop and the nucleotide binding loop. These coincided with changes apparent in Fig. 2 and are similar to movements observed with other protein kinases [51].

The active conformation KIT models presented here contain ATP docked in by hand and the resulting complex energy minimised using Tripos software. The structural changes upon activation resulted in the ATP binding site being slightly smaller and tighter and the cleft between the N- and C-terminal lobes being closed (Fig. 2). The Gly-rich loop, a flexible segment of the nucleotide binding loop, is 4 Å closer to the C-terminal lobe in the inactive conformation than in the active conformation. It anchors the β and γ phosphates of ATP to orientate it for catalysis, and is partially obscured by the first section of the activation loop in the inactive conformation. Mutations in the Gly-rich loop have been shown to decrease kinase activity [54–56].

Some of the contacts between ATP and KIT kinase are subtly different from those in IRK_a (see Table 3). As in the template crystal structure, the adenine system of ATP is bound in a hydrophobic pocket. The structure of the catalytic loop is very similar to the template IRK_a in our KIT_a models, positioning ATP correctly with respect to the catalytic residues for phosphorylation of a substrate protein. The movement of the αC helix closer into the binding pocket upon activation enables an ion pair formation between conserved Glu640 (in the αC helix) and Lys623 side chains (in the nucleotide binding loop). This allows the interaction of Lys623 with the phosphates of ATP. As observed in the insulin receptor crystal structures, Phe811 and Gly812 of the conserved Asp-Phe-Gly motif move out of the ATP binding site upon ATP binding, while the side chain of Asp810 moves into the binding site.

Table 2
Energy differences associated with conformational changes in wild-type and Val816 mutant KIT models

Conformational change	Change in energy[a] (kcal/mol)	
	Asp816KIT	Val816KIT
Activation only	2189	−188
ATP binding to active form	−1202	−2507
Phosphorylation of active form	−362	−120
Phosphorylation of inactive form	−80	−209

[a] Negative value means the conformational change is favoured.

The large, flexible activation loop begins at the conserved Asp-Phe-Gly residues and ends at the conserved Ala-Phe-Glu sequence. In the active conformation the whole loop is flexed into an open and extended conformation away from the ATP binding pocket. In other tyrosine kinases the conformation of the activation loop is controlled by phosphorylation of specific tyrosine residues [57]. In KIT this segment contains only one tyrosine (Tyr823) located at the end of the activation loop. In our active conformation models we saw no obvious difference to the structure on phosphorylation of Tyr823, although it was energetically favourable (Table 2), suggesting that this phosphorylation event is not the major driving force for the switch to the active conformation in KIT. In Asp816KIT_i, Tyr823 forms three hydrogen bonds with residues of the P + 1 loop. Thus, in the inactive conformation of KIT, the substrate binding P + 1 loop is partially blocked by Tyr823 of the activation loop, which mimics substrate binding. These self-inhibitory interactions [58] are relieved in the active conformations. In Asp816KIT_a these hydrogen bonds change and the P + 1 loop is freed. Phosphorylation of Tyr823 does not change the hydrogen bonds in the active conformation model. Rather, the conformation of the activation loop in KIT seems to be controlled by hydrogen bonds of other activation loop residues (see below).

3.4. The Asp816Val mutation and its effect upon activation of KIT

Residue 816, like Tyr823, is located in a section of the activation loop that moves dramatically away from the ATP binding pocket upon activation. Asp816 stabilises the activation loop in an inactive conformation via two hydrogen bonds (Fig. 4a, Table 3) to the peptide backbone of Lys818 and Asn819. One of these, importantly, involves the Asp816 side chain. ATP binding disrupts these

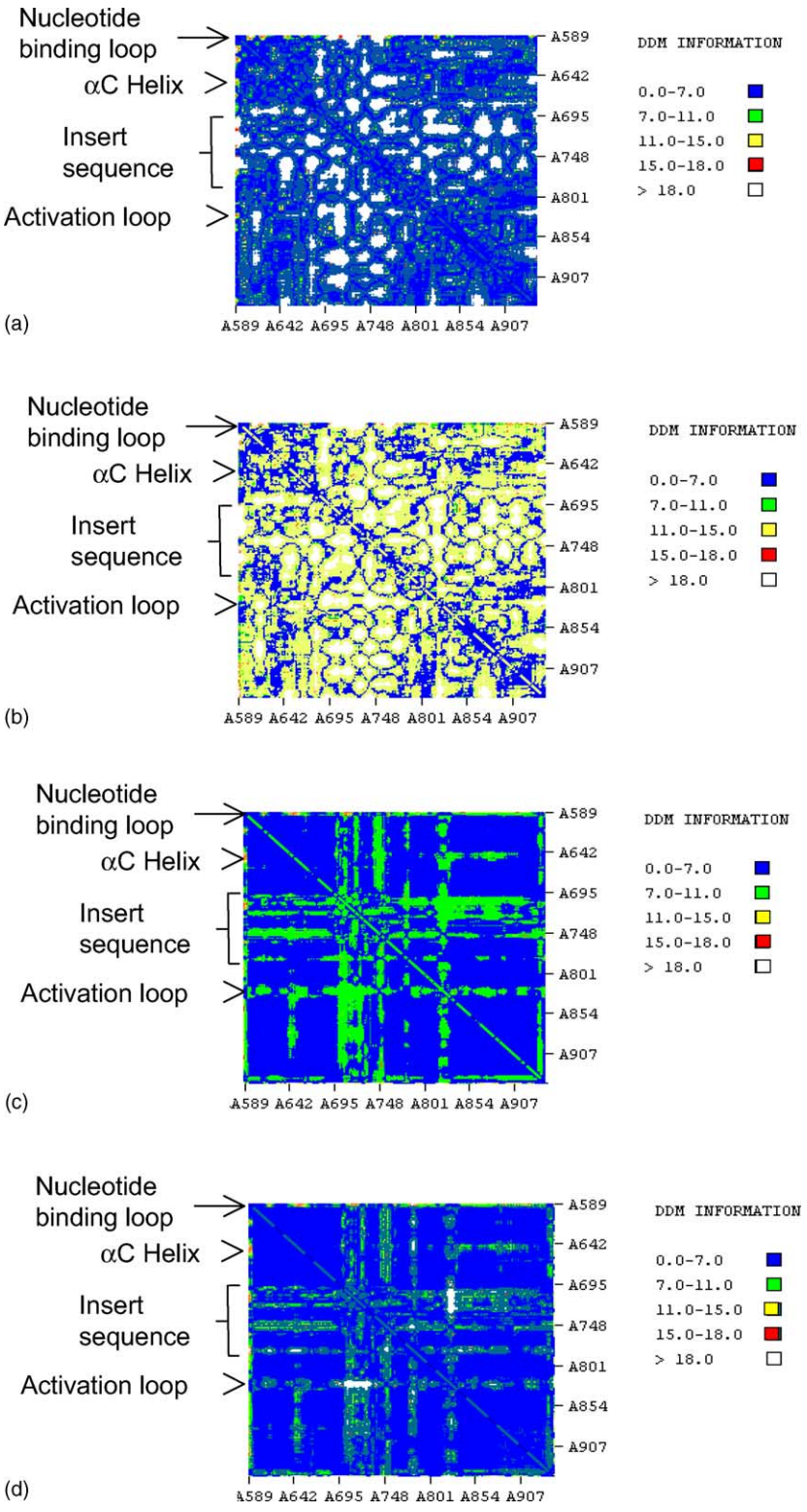

Fig. 3. Difference Distance matrices (DDMs) obtained from ProFlex. This program measures the distances between all pairs of Cα atoms of a structure and then compares the resulting matrices for the two structures and constructs a DDM. The DDMs are colour-coded according to the magnitude of the differences observed between the two structures (in Å). All four KIT models were compared with one another: (a) Asp816KIT_i vs. Asp816KIT_a (b) Asp816KIT_a vs. Val816KIT_a (c) Asp816KIT_i vs. Val816KIT_a (d) Val816KIT_i vs. Val816KIT_a.

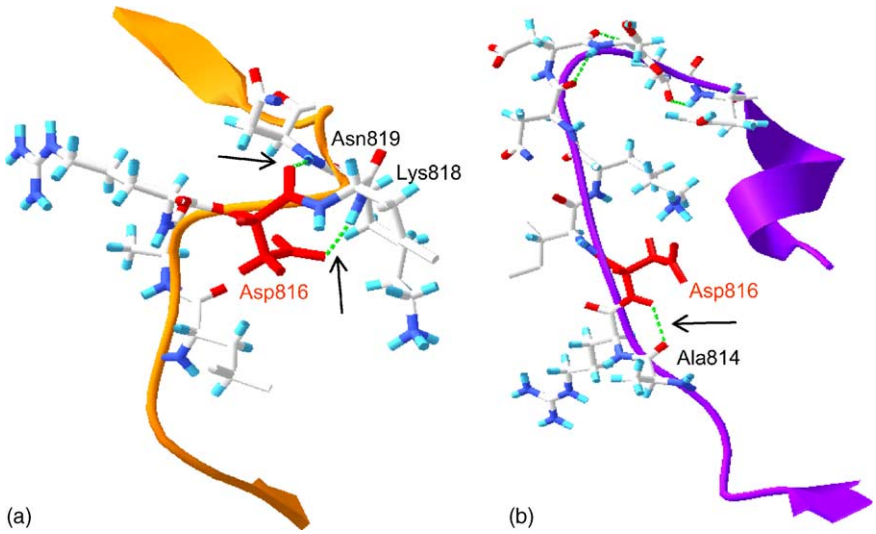

Fig. 4. Detail of the activation loop around residue 816 (in red). Backbones are shown as ribbons, all sidechain atoms are depicted, colour coded by element (white: C; blue: N; red: O; green: H). (a) Asp816KIT_i model: Asp816 stabilises the activation loop conformation by forming two hydrogen bonds (green dashed lines) with Lys818 and Asn819; (b) Asp816KIT_a model: Asp816 forms one hydrogen bond with Ala814. Lys818 and Asn819 form different hydrogen bonds to stabilise the active conformation of the activation loop.

hydrogen bonds, causing the dramatic movement of the activation loop, which flexes into an open and extended conformation away from the ATP binding pocket (see Fig. 2d). The side chain of the equivalent residue in the inactive insulin conformation (IRK_i) is not resolved in the crystal structure. However, SWISS-MODEL adds this and other unresolved side chains and this then enables the Asp residue to form four hydrogen bonds, two of which are to equivalent residues to Lys818 and Asn819 of KIT. Each of these proposed hydrogen bonds involves one resolved backbone partner, which increases their likelihood. IRK_a (all side chains resolved in the crystal structure) maintains only one of these hydrogen bonds, but gains another different hydrogen bond, resulting in a potential net loss of two hydrogen bonds upon activation. In the inactive ABL conformation, the backbone of the Leu387 residue, equivalent to Asp816 in KIT, also forms a local hydrogen bond (with the Leu384 backbone), as does the Met388 backbone. Thus, the stabilisation of this part of the activation loop via local hydrogen bonds is common in the inactive conformations of several kinases and explains at least in part why mutation at this point disrupts the inactive kinase conformation.

While mutation of Asp816 to Val816 causes a loss of hydrogen bonds in the model of inactive KIT, the physical changes upon activation are much the same in the mutant and the wild type models, although the details of many interactions differ. For example, the loss of self-inhibition is complete for the Val816KIT_a model and all contacts between the activation loop and the P + 1 loop are lost. In both mutant models different hydrogen bonds are formed that partially compensate for a loss of the hydrogen bonds involving Asp816 in the wild type models (see Table 3).

From Table 2, it can be seen that the active conformation (without ATP bound) of the mutant is more stable than the inactive conformation, whereas the reverse is true for wild-type KIT. In both cases, the binding of ATP stabilises the active conformation considerably. The phosphorylation of Tyr823 also stabilises the active conformations somewhat, however it also stabilises the inactive conformations of both KIT models. This suggests that ATP binding and not phosphorylation of Tyr823 is the important step in the adoption of the active conformation of the KIT kinase domain. Overall, the three events of conformational change, ATP binding and phosphorylation of Tyr823 in the Val816 mutant lead to a much more stable structure (by 2815 kcal/mol), whereas for the wild type KIT these events lead to a destabilization of the kinase domain by 625 kcal/mol. This could possibly explain why ligand-induced dimerisation and conformational changes in the juxtamembrane region are essential for normal KIT signalling, but are not required for activity for the Val816 mutant, which displays constitutive activity. The current models of the kinase domain do not allow assessment of the energetic and structural impact of ligand binding and dimerisation on the whole receptor protein.

3.5. Comparison of active conformation models to the KIT kinase domain crystal structure

A crystal structure of the active conformation of the juxtamembrane and kinase regions of KIT was recently reported, and although the paper gives little detail [59], the atomic coordinates are now publicly available (pdb code 1 pkg). The residues of the kinase insert are disordered and no coordinates are given for them.

The overall structure is identical to our KIT_a models and several interactions, such as the salt bridge between Glu640 of the αC helix and Lys623, are the same. Other interactions are slightly different, such as the environment of the

Table 3
Hydrogen bonds observed in the KIT crystal structure and the models

	KIT_a	Asp816KIT_I	Asp816KIT_a	Val816KIT_I	Val816KIT_a
GxGxxG					
Gly596	Val603	Val603 (2x)	Val603 (2x)	Val603 (2x)	Val603
Ala597	–	–	–	–	
Gly598	–	Gly601 (2x)	Gly601 (2x)	Gly601 (2x)	Water, ATP
Ala599	–	Phe811	–	Phe811	Water
Phe600	ANP	Lys626	Lys626	Lys626	Gly601
Gly601	ANP	Gly598 (2x)	Gly598 (2x)	Gly598 (2x)	Lys626
Catalytic loop					
Asn787	Leu783, Ala784, Ile817	Ala784	Ser785, Ala794	Ala784, Ser785	Ala784, Ile817
Cys788	Leu783	Leu783	Leu783	Leu783	Leu783, Lys786
Ile789	Arg815 (2x)	–	–	Ser771(2x), Arg791	Arg815
His790	Asp792, Leu793, Cys809, Asp810, Asp851	Asp792, Asp851	Asp792, Gly812, Asp851	Arg791, Asp851	Asp851, Water
Arg791	Leu813, Asp851	Leu793, Asp851	Leu793, Asp851	Ile789, His790	Leu813,Tyr846, Asp851
Asp792	Ala794, Arg796, Asn797	His790, Ala794, Arg796 (3x)	His790, Ala794, Arg 796 (4x)	Arg796 (3x)	Ala794, Arg796 (3x)
Leu793	His790	Arg791	Arg791	–	Ser854
Ala794	Asp792, Asn797	Asp792, Asn797	Asp792, Asn797	Asn797	Asp792,Asn797
Ala795	Leu679, Glu861	Leu679, Glu861	Ile798, Glu861	Leu679, Glu861	Glu861 (2x)
Arg796	Asp792, ANP	Asp792 (3x)	Asp792 (4x)	Asp792 (3x)	Asp792 (3x)
Asn797	Asp792, Ala794, Cys809(2x), Asp810, ANP	Ala794, Cys809	Ala794, Cys809	Ala794	Ala794, Cys809
Activation loop					
Asp810	His790, Asn797, ANP	Gly812, Leu813	–	Val776, Gly812, Leu813	Gly812
Phe811	Glu640	Ala599	–	Ala599	Ala814
Gly812	–	Asp810, Ala814	–	Asp810, Ala814	Asp810, Arg815
Leu813	Arg791	Asp810	His790	Asp810	Arg791
Ala814	Arg815	Gly812	Asp816	Gly812	Arg815
Arg815	Ile789(2x), Ala814, Tyr823	–	–	–	Ile789, Gly812 (2x), Ala814
816	Ile817, Lys818	Lys818, Asn819	Ala814	Asn819	–
Ile817	Asn787, Asp816	–	–	–	Asn787, Ser821
Lys818	Asp816	Asp816, Ser821	–	Ser821	Asp820
Asn819	–	Asp816, Asp820	Ser821	Val816, Asn822	–
Asp820	Ile817	Ser821, Ser868	Asn822	Ser821(2x), Ser868	Lys818, Asn822
Ser821	Tyr823	Lys818, Asp820	Asn819	Lys818, Asp820(2x)	Ile817
Asn822	–	Asn819, Arg830	Asp820, Tyr823	Asn819, Arg830	Asp820,Tyr823, Tyr846
Tyr823	Ser821, Tyr846(2x)	Val825, Leu831 (2x)	Asn822	Val825, Leu831(2x), Asp876	Asn822, Tyr846 (2x)
Val824	Lys826(w), Cys844	Gly827, Asn828	Asn828	Gly827	–
Val825	Cys844	Tyr823, Asn828, Ala829	Ala829	Tyr823, Asn828, Ala829	–
Lys826	Val824(w)	–	Arg830	–	–
Gly827	–	Val824	–	Val824	–
P + 1 loop					
Asn828	–	Val824, Val 825	Val824	Val825	–
Ala829	–	Val825	Val825	Val825, Leu831	Leu831
Arg830	–	Asn819(2x),Asn822	Lys826, Val875	Asn822	Glu633 (2x)
Leu831	Val833	Tyr823(2x), Val833	Val833	Tyr823(2x), Ala829, Val833	Ala829, Val833
Pro832	Trp835	Trp835	Trp835	Trp835, Met836	Trp835
Val833	Leu831, Met836	Leu831, Met836	Leu831, Met836	Leu831, Met836	Leu831, Met836
Lys834	–	–	–	–	–
Trp835	Pro832, Ser854, Glu861	Pro832	Pro832	Trp853	Pro832
Met836	Val833	Val833	Val833	Pro832, Val833	Val833
Ala837	Ser840, Ile841(w)	Ile841	Ile841	Ile841	Ser840, Ile841

(w): denotes weak hydrogen bond.

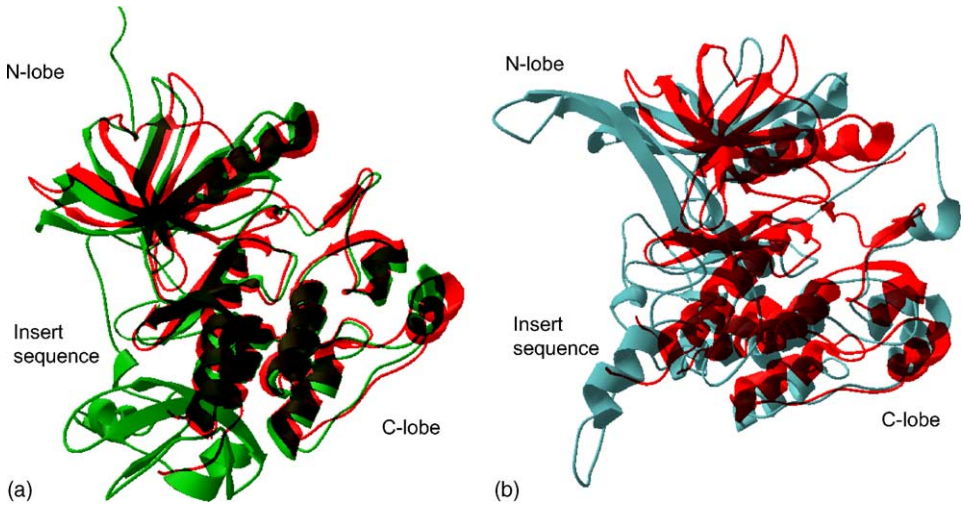

Fig. 5. Superimposition of the KIT crystal structure (red) onto the KIT_a models (green): (a) Val816KIT_a (b) Asp816KIT_a.

conserved Asp-Phe-Gly motif at the start of the activation loop (Table 3). We docked ATP into our models, whereas the crystal structure contains ADP, so it is not surprising to find somewhat different interactions for the phosphate groups and the coordination of the Mg^{2+}. However, the overall orientation of the ligand is the same.

The most striking finding, however, is the very close correspondence between our mutant model, Val816KIT_a, and this crystal structure (Fig. 5a). The C-lobe of our wild-type model, Asp816KIT_a, also overlays well with the crystal structure (Fig. 5b). The N-lobe of our wild-type model, however, is rotated relative to the crystal structure. The detailed interactions listed in Table 3 also confirm that, particularly for the activation loop, the Val816KIT_a model is closer to the crystal structure than the Asp816KIT_a model. The mutant model of the active conformation is also much lower in energy than the wild-type model (see Table 1) and together, these findings suggest that the wild-type kinase domain is strongly influenced by other regions of the entire protein, such as the juxtamembrane domain, whereas the Asp816Val

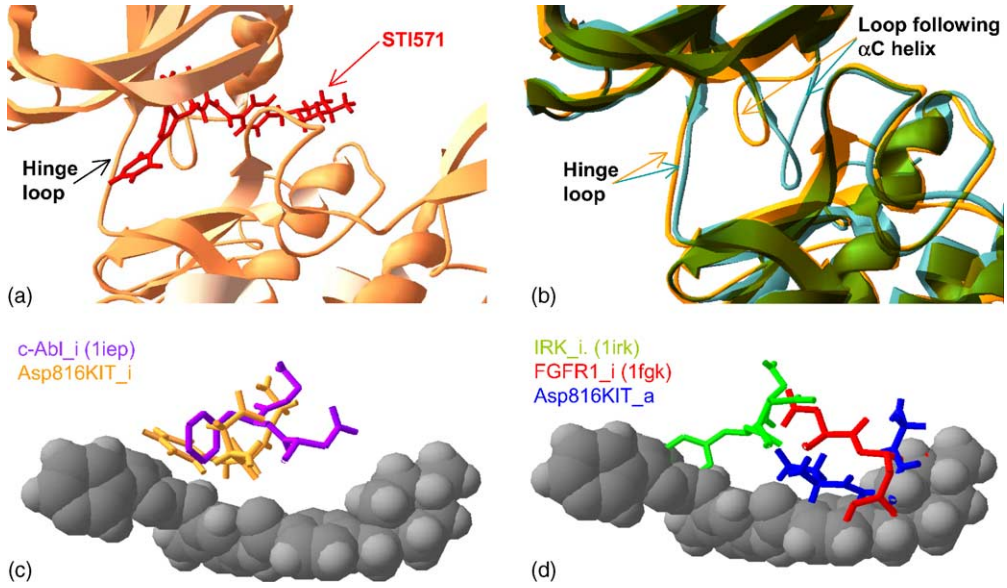

Fig. 6. (a) Detail of the ATP binding site of the Asp816KIT_i model (orange ribbon trace of backbone) with STI571 (in red) docked in. (b) Same as (a), superimposed with the crystal structure IRK_i (green). (c) Detail of STI571 (grey spacefilling rendering of all atoms) docked into the Asp816KIT_i model. Only the side chains of the residues of the conserved Asp-Phe-Gly motif are shown in orange for the Asp816KIT_i model and in purple for the ABL_i crystal structure in complex with STI571 superimposed onto the KIT model (STI571 from the crystal structure not shown), explaining in part why STI571 is able to bind to both KIT_i and ABL_i. (d) Detail of STI571 (grey spacefilling rendering of all atoms) docked into the Asp816KIT_i model. Only the side chains of the residues of the conserved Asp-Phe-Gly motif are shown in green for the IRK_i crystal structure, in red for the FGFR1_i crystal structure and in blue for the model of the active conformation of KIT superimposed onto the Asp816KIT_i model, explaining in part why STI571 is not able to bind to IRK, FGFR1 or the active conformation of KIT.

mutant kinase domain is able to fold into an active conformation in isolation.

3.6. Binding of the kinase inhibitor STI571 to the KIT models

STI571 is an ATP-competitive kinase inhibitor active on ABL, PDGFRα, PDGFRα and β but devoid of significant activity against most other kinases, including the insulin receptor. To elucidate the selectivity of STI571 binding for certain kinases, it was docked into our models guided by the STI571-ABL co-crystal structure and the resulting complexes were refined by energy minimization as described above. Fig. 6a and c illustrates our model Asp816KIT_i in complex with STI571 and shows that the large, open ATP binding site allows the inhibitor, which is considerably larger than ATP, to be docked in. STI571 binds to KIT via only two hydrogen bonds and sits in a very hydrophobic pocket: the pyridine-N forms a hydrogen bond to Cys673 and a second nitrogen of STI571 forms a hydrogen bond to the side chain OH group of Thr670. There is one β-cation interaction between the central phenyl ring of the inhibitor and the Lys623 side chain of Asp816KIT_i. By comparison, on binding to ABL in the crystal structure STI571 forms three hydrogen bonds. The inhibitor could not be fitted into the active conformation models due to the 'tightening' of the binding site (Fig. 6d).

Comparison of the KIT kinase model with the IRK_i crystal structure (Fig. 6b) reveals two loops, the hinge loop (after β5) and a loop following the αC helix, protruding further into the ATP binding site for IRK. Furthermore, the conserved Asp-Phe-Gly motif at the start of the activation loop is folded differently for kinases, such as IRK and FGFR1, which are not inhibited by STI571 (Fig. 5d). Similar collisions of the Asp-Phe-Gly motif with the position where STI571 binds in the ABL_i crystal structure and our Asp816KIT_i model are also observed for HCK and LCK (data not shown), explaining, at least in part, the inability of STI571 to bind to IRK, FGFR1, HCK, and LCK. This finding is interesting in light of the fact that the IRK_i structure was used as the template for our modelling. Additionally, we show that the active conformation of KIT also places the Asp-Phe-Gly motif in a position where it interferes with STI571 binding (Fig. 6d). In Asp816KIT_i and in the ABL_i crystal structure complexed with STI571, this motif, and in particular the Phe side chain, is rotated out of the binding pocket (Fig. 6c).

4. Discussion

We have used homology modelling of the active and inactive conformations of the KIT RTK to examine receptor activation and inhibitor sensitivity.

Our homology models lead us to suggest that phosphorylation of the Tyr823 residue of the receptor tyrosine kinase KIT is not the driving force in attaining an active conformation capable of phosphorylation of substrate proteins. This conclusion has independently been reached based on the crystal structure of KIT complexed with ADP [59]. Their study found that in this active conformation Tyr823 is not phosphorylated and, furthermore, phosphorylation site mapping experiments localised the first two phosphorylation sites to two Tyr residues in the juxtamembrane domain. The data also suggest that Tyr823 is one of the last Tyr to be phosphorylated. This is in contrast to most other kinases which have more than one Tyr in the activation loop, where phosphorylation of those Tyr residues is required for the kinase active conformation to be attained [6]. It has been known for some time that Tyr823 (Tyr821 in murine Kit) is not essential for KIT kinase activity [60].

Our molecular modelling studies comparing the active and inactive conformations of KIT provide an explanation for the constitutive activation by mutations resulting in substitutions at position 816 in the activation loop. We show that the Asp residue at position 816 stabilises the inactive conformation of the kinase domain by forming hydrogen bonds with the Lys818 and Asn819 backbone. These bonds are lost when Asp816 is replaced by a different amino acid. Energy calculations indicate that the Asp816Val substitution also stabilises the structure in its active form. Thus, this mutation favours the transition from the inactive to the active conformation of the KIT kinase domain by destabilising the activation loop, freeing the steric hindrances that prevent the rearrangements of the two lobes and thereby allowing other critical movements associated with kinase activation. This loss of constraints allows αC helix movement and the correct positioning of residues in and from the active site. In the mutant form, energy calculations indicate that the active conformation bound to ATP is extremely stable relative to the wild-type receptor. This suggests that higher order interactions such as dimerisation or altered interactions with other parts of the protein (e.g. the juxtamembrane region) are not required to drive activation of Asp816Val KIT. Our model of the activated isolated kinase domain of Asp816Val KIT is identical to the recently published crystal structure [59]. In this crystal structure the phosphorylated juxtamembrane domain of an adjacent enzyme molecule is inserted between the activation loop and the C-lobe and this may stabilise the active conformation of the activation loop. The juxtamembrane domain may thus not only fulfil an autoinhibitory role when unphosphorylated [13,14], but, when phosphorylated, may also be involved in stabilisation of the active conformation. Since our model of the wild-type 'active conformation' of KIT does not contain the juxtamembrane domain, parts of the N-lobe, in particular, are not folded correctly, when compared to the crystal structure. Experimental evidence on the importance of dimerisation and the juxtamembrane domain for activity of this mutant is inconclusive. The initial report suggested that dimerisation was not required for the constitutive activity of the homologous mutant (Asp814Tyr) murine Kit [61]. However, more recently experiments with

dominant negative kinase mutants as well as biochemical studies with isolated recombinant Kit intracellular domains have indicated that the Asp814 mutation promotes dimer formation independent of the extracellular domain, and requires dimerisation for full activity [62,63]. This may result from a requirement for dimer formation for receptor transphosphorylation, as has also been suggested by Mol et al. [59]. While the crystal structure suggests an important role for the juxtamembrane domain in activation of KIT, investigations by Chan et al. [13] on recombinant forms of Kit found that mutation or deletion of this domain lead to extremely rapid activation kinetics. Furthermore, disruptions of this region by duplicate deletions or point mutations lead to constitutive activity and commonly occur in GIST [18,19,33,34].

While the replacement of Asp816 with Val is the most commonly observed activating mutation at this position, other substitutions have been observed in specimens from patients with systemic mastocytosis (Asp816Tyr; Asp816Phe; [64]) and acute myeloid leukaemia (Asp816Tyr, [16]; Asp816Asn, [17]). These and other substitutions e.g. Asp816His in human KIT or at the corresponding positions in rodent Kit, have been identified in cell lines and shown to result in constitutive Kit phosphorylation and factor-independent growth [17,65]. Moriyama et al. [66] systematically replaced Asp814 of murine Kit with all other amino acids and found that all except Asp814Cys displayed ligand-independent autophosphorylation, and most displayed enhanced in vitro kinase activity. Consistent with our model, these data indicate that the loss of Asp816, rather than a particular substituent, is responsible for constitutive activation.

The Asp residue corresponding to position 816 in KIT is highly conserved in many RTKs suggesting that mutation of this residue is a common mechanism of activation of related receptors. Indeed, mutations in the corresponding Asp residue of other RTKs have been observed in malignancies including Asp835 in FLT3 [67] and Asp1228 in MET [68]. Recent evidence has demonstrated that 5–10% of AML patients display a mutated Asp835 residue in FLT3, implicating it in development of AML and identifying it as an important target for inhibitors. Similar molecular modelling like that shown here for KIT can be utilised for understanding the mechanism of activation and for analysing the binding potential of inhibitors to mutant FLT3 receptors.

With the success of STI571 as a targeted cancer therapeutic, the development of new tyrosine kinase inhibitors is expanding rapidly [69–72]. So far, the most effective compounds, like STI571, bind to the ATP-binding region with selectivity for the target protein [73]. STI571 has been shown to inhibit BCR/ABL kinase activity by trapping the kinase domain into the inactive conformation [74]. Similarly, in our model of the KIT kinase domain, STI571 could only be accommodated in the inactive configuration. We also demonstrated that in STI571 insensitive kinases such as IRK, various loops protrude into the putative inhibitor binding site, in particular the conserved Asp-Phe-Gly segment at the beginning of the activation loop. The active configuration of the KIT kinase domain is strongly favoured in Asp816Val mutant form, providing an explanation for why the inhibitor is inactive on this form of KIT [31,32]. Similarly, the Asp816Phe and Asp816Tyr mutants were shown to be resistant to STI571 [31]. Many different mutations in the BCR/ABL kinase domain, including non-contact residues, give rise to resistance [38,39,75] and several of these also bring about enhanced kinase activity suggesting that a similar mechanism may apply.

Most, but not all, of the kinase inhibitors under evaluation target the inactive conformation. Because the similarity between the active conformations of protein tyrosine kinases is greater than the similarity between the inactive conformations, this results in better selectivity for the target kinase [6], an important attribute for clinical use [76]. However, it now appears that such selectivity is likely to come at the expense of resistance due to development of mutations that, like Asp816Val in KIT, strongly favour the active conformation. Use of combinations of kinase inhibitors capable of interacting with different conformations and/or mutant forms of the target may overcome the problem of the emergence of resistance as a result of drug exposure. For example, in contrast to STI571, PD173955 binds to a conformation of ABL in which the activation loop resembles that of an active kinase [47].

5. Conclusions

We have shown that in the absence of crystal structures of target kinases in multiple liganded and unliganded states, homology modelling of the kinase domain based on similar structures can explain how mutations give rise to constitutive activation and/or drug resistance. This approach can be used in studies of other clinically important protein tyrosine kinases such as FLT-3, and will be valuable in designing new selective inhibitors. Thus, structural analysis based on computational methods is now, even more than before, an important part of drug design [77].

References

[1] Y. Yarden, W.J. Kuang, T. Yang-Feng, L. Coussens, S. Munemitsu, T.J. Dull, E. Chen, J. Schlessinger, U. Francke, A. Ullrich, Human proto-oncogene c-kit: a new cell surface receptor tyrosine kinase for an unidentified ligand, EMBO J. 6 (1987) 3341–3351.
[2] F. Qiu, P. Ray, K. Brown, P. Barker, S. Jhanwar, F. Ruddle, P. Besmer, Primary structure of c-kit: relationship with the CSF-1/PDGF receptor kinase family—oncogenic activation of v-kit involves deletion of extracellular domain and C terminus, EMBO J. 7 (1988) 1003–1011.
[3] A. Ullrich, J. Schlessinger, Signal transduction by receptors with tyrosine kinase activity, Cell 61 (1990) 203–212.
[4] L.K. Ashman, The biology of stem cell factor and its receptor C-kit, Int. J. Biochem. Cell Biol. 31 (1999) 1037–1051.
[5] S.R. Hubbard, M. Mohammadi, J. Schlessinger, Autoregulatory mechanisms in protein-tyrosine kinases, J. Biol. Chem. 273 (1998) 11987–11990.

[6] M. Huse, J. Kuriyan, The conformational plasticity of protein kinases, Cell 109 (2002) 275–282.
[7] J. Schlessinger, Cell signaling by receptor tyrosine kinases, Cell 103 (2000) 211–225.
[8] S.K. Hanks, T. Hunter, Protein kinases 6. The eukaryotic protein kinase superfamily: kinase (catalytic) domain structure and classification, FASEB J. 9 (1995) 576–596.
[9] M. Mohammadi, G. McMahon, L. Sun, C. Tang, P. Hirth, B.K. Yeh, S.R. Hubbard, J. Schlessinger, Structures of the tyrosine kinase domain of fibroblast growth factor receptor in complex with inhibitors, Science 276 (1997) 955–960.
[10] M.A. McTigue, J.A. Wickersham, C. Pinko, R.E. Showalter, C.V. Parast, A. Tempczyk-Russell, M.R. Gehring, B. Mroczkowski, C.C. Kan, J.E. Villafranca, K. Appelt, Crystal structure of the kinase domain of human vascular endothelial growth factor receptor 2: a key enzyme in angiogenesis, Struct. Fold Des. 7 (1999) 319–330.
[11] S.R. Hubbard, Crystal structure of the activated insulin receptor tyrosine kinase in complex with peptide substrate and ATP analog, EMBO J. 16 (1997) 5572–5581.
[12] L.K. Ashman, P. Ferrao, S.R. Cole, A.C. Cambareri, Effects of mutant c-Kit in early myeloid cells, Leuk. Lymphoma 34 (1999) 451–461.
[13] P.M. Chan, S. Ilangumaran, J. La Rose, A. Chakrabartty, R. Rottapel, Autoinhibition of the kit receptor tyrosine kinase by the cytosolic juxtamembrane region, Mol. Cell Biol. 23 (2003) 3067–3078.
[14] L.E. Wybenga-Groot, B. Baskin, S.H. Ong, J. Tong, T. Pawson, F. Sicheri, Structural basis for autoinhibition of the Ephb2 receptor tyrosine kinase by the unphosphorylated juxtamembrane region, Cell 106 (2001) 745–757.
[15] H. Nagata, A.S. Worobec, C.K. Oh, B.A. Chowdhury, S. Tannenbaum, Y. Suzuki, D.D. Metcalfe, Identification of a point mutation in the catalytic domain of the protooncogene c-kit in peripheral blood mononuclear cells of patients who have mastocytosis with an associated hematologic disorder, Proc. Natl. Acad. Sci. U.S.A. 92 (1995) 10560–10564.
[16] A. Beghini, R. Cairoli, E. Morra, L. Larizza, In vivo differentiation of mast cells from acute myeloid leukemia blasts carrying a novel activating ligand-independent C-kit mutation, Blood Cells Mol. Dis. 24 (1998) 262–270.
[17] Z.Q. Ning, J. Li, R.J. Arceci, Activating mutations of c-kit at codon 816 confer drug resistance in human leukemia cells, Leuk. Lymphoma 41 (2001) 513–522.
[18] M.C. Heinrich, B.P. Rubin, B.J. Longley, J.A. Fletcher, Biology and genetic aspects of gastrointestinal stromal tumors: KIT activation and cytogenetic alterations, Hum. Pathol. 33 (2002) 484–495.
[19] S. Hirota, K. Isozaki, Y. Moriyama, K. Hashimoto, T. Nishida, S. Ishiguro, K. Kawano, M. Hanada, A. Kurata, M. Takeda, G. Muhammad Tunio, Y. Matsuzawa, Y. Kanakura, Y. Shinomura, Y. Kitamura, Gain-of-function mutations of c-kit in human gastrointestinal stromal tumors, Science 279 (1998) 577–580.
[20] Q. Tian, H.F. Frierson Jr., G.W. Krystal, C.A. Moskaluk, Activating c-kit gene mutations in human germ cell tumors, Am. J. Pathol. 154 (1999) 1643–1647.
[21] T. Hongyo, T. Li, M. Syaifudin, R. Baskar, H. Ikeda, Y. Kanakura, K. Aozasa, T. Nomura, Specific c-kit mutations in sinonasal natural killer/T-cell lymphoma in China and Japan, Cancer Res. 60 (2000) 2345–2347.
[22] K. Hibi, T. Takahashi, Y. Sekido, R. Ueda, T. Hida, Y. Ariyoshi, H. Takagi, Coexpression of the stem cell factor and the c-kit genes in small-cell lung cancer, Oncogene 6 (1991) 2291–2296.
[23] S.J. Hines, C. Organ, M.J. Kornstein, G.W. Krystal, Coexpression of the c-kit and stem cell factor genes in breast carcinomas, Cell Growth Differ. 6 (1995) 769–779.
[24] G.W. Krystal, S.J. Hines, C.P. Organ, Autocrine growth of small cell lung cancer mediated by coexpression of c-kit and stem cell factor, Cancer Res. 56 (1996) 370–376.
[25] G.W. Krystal, S. Honsawek, D. Kiewlich, C. Liang, S. Vasile, L. Sun, G. McMahon, K.E. Lipson, Indolinone tyrosine kinase inhibitors block Kit activation and growth of small cell lung cancer cells, Cancer Res. 61 (2001) 3660–3668.
[26] R.S. DiPaola, W.I. Kuczynski, K. Onodera, M.Z. Ratajczak, N. Hijiya, J. Moore, A.M. Gewirtz, Evidence for a functional kit receptor in melanoma, breast, and lung carcinoma cells, Cancer Gene Ther. 4 (1997) 176–182.
[27] R. Vitali, V. Cesi, M.R. Nicotra, H.P. McDowell, A. Donfrancesco, O. Mannarino, P.G. Natali, G. Raschella, C. Dominici, c-Kit is preferentially expressed in MYCN-amplified neuroblastoma and its effect on cell proliferation is inhibited in vitro by STI-571, Int. J. Cancer 106 (2003) 147–152.
[28] E. Buchdunger, C.L. Cioffi, N. Law, D. Stover, S. Ohno-Jones, B.J. Druker, N.B. Lydon, Abl protein-tyrosine kinase inhibitor STI571 inhibits in vitro signal transduction mediated by c-kit and platelet-derived growth factor receptors, J. Pharmacol. Exp. Ther. 295 (2000) 139–145.
[29] B.J. Druker, C.L. Sawyers, H. Kantarjian, D.J. Resta, S.F. Reese, J.M. Ford, R. Capdeville, M. Talpaz, Activity of a specific inhibitor of the BCR-ABL tyrosine kinase in the blast crisis of chronic myeloid leukemia and acute lymphoblastic leukemia with the Philadelphia chromosome, N. Engl. J. Med. 344 (2001) 1038–1042.
[30] B.J. Druker, M. Talpaz, D.J. Resta, B. Peng, E. Buchdunger, J.M. Ford, N.B. Lydon, H. Kantarjian, R. Capdeville, S. Ohno-Jones, C.L. Sawyers, Efficacy and safety of a specific inhibitor of the BCR-ABL tyrosine kinase in chronic myeloid leukemia, N. Engl. J. Med. 344 (2001) 1031–1037.
[31] Y. Ma, S. Zeng, D.D. Metcalfe, C. Akin, S. Dimitrijevic, J.H. Butterfield, G. McMahon, B.J. Longley, The c-KIT mutation causing human mastocytosis is resistant to STI571 and other KIT kinase inhibitors kinases with enzymatic site mutations show different inhibitor sensitivity profiles than wild-type kinases and those with regulatory-type mutations, Blood 99 (2002) 1741–1744.
[32] M.J. Frost, P.T. Ferrao, T.P. Hughes, L.K. Ashman, Juxtamembrane mutant V560GKit is more sensitive to Imatinib (STI571) compared with wild-type c-kit whereas the kinase domain mutant D816VKit is resistant, Mol. Cancer Ther. 1 (2002) 1115–1124.
[33] M. Taniguchi, T. Nishida, S. Hirota, K. Isozaki, T. Ito, T. Nomura, H. Matsuda, Y. Kitamura, Effect of c-kit mutation on prognosis of gastrointestinal stromal tumors, Cancer Res. 59 (1999) 4297–4300.
[34] H. Chen, K. Isozaki, K. Kinoshita, A. Ohashi, Y. Shinomura, Y. Matsuzawa, Y. Kitamura, S. Hirota, Imatinib inhibits various types of activating mutant kit found in gastrointestinal stromal tumors, Int. J. Cancer 105 (2003) 130–135.
[35] B.J. Longley, M.J. Reguera, Y. Ma, Classes of c-KIT activating mutations: proposed mechanisms of action and implications for disease classification and therapy, Leuk. Res. 25 (2001) 571–576.
[36] G.D. Demetri, Targeting the molecular pathophysiology of gastrointestinal stromal tumors with imatinib. Mechanisms, successes, and challenges to rational drug development, Hematol. Oncol. Clin. North Am. 16 (2002) 1115–1124.
[37] R. Dagher, M. Cohen, G. Williams, M. Rothmann, J. Gobburu, G. Robbie, A. Rahman, G. Chen, A. Staten, D. Griebel, R. Pazdur, Approval summary: imatinib mesylate in the treatment of metastatic and/or unresectable malignant gastrointestinal stromal tumors, Clin. Cancer Res. 8 (2002) 3034–3038.
[38] M.E. Gorre, M. Mohammed, K. Ellwood, N. Hsu, R. Paquette, P.N. Rao, C.L. Sawyers, Clinical resistance to STI-571 cancer therapy caused by BCR-ABL gene mutation or amplification, Science 293 (2001) 876–880.
[39] N.P. Shah, J.M. Nicoll, B. Nagar, M.E. Gorre, R.L. Paquette, J. Kuriyan, C.L. Sawyers, Multiple BCR-ABL kinase domain mutations confer polyclonal resistance to the tyrosine kinase inhibitor imatinib (STI571) in chronic phase and blast crisis chronic myeloid leukemia, Cancer Cell 2 (2002) 117–125.
[40] T. Furitsu, T. Tsujimura, T. Tono, H. Ikeda, H. Kitayama, U. Koshimizu, H. Sugahara, J.H. Butterfield, L.K. Ashman, Y. Kanayama, et al., Identification of mutations in the coding sequence

of the proto-oncogene c-kit in a human mast cell leukemia cell line causing ligand-independent activation of c-kit product, J. Clin. Invest. 92 (1993) 1736–1744.
[41] D.G. Higgins, J.D. Thompson, T.J. Gibson, Using CLUSTAL for multiple sequence alignments, Methods Enzymol. 266 (1996) 383–402.
[42] N. Guex, M.C. Peitsch, SWISS-MODEL and the Swiss-PdbViewer: an environment for comparative protein modeling, Electrophoresis 18 (1997) 2714–2723.
[43] S.J. Hubbard, F. Eisenmenger, J.M. Thornton, Modeling studies of the change in conformation required for cleavage of limited proteolytic sites, Protein Sci 3 (1994) 757–768.
[44] M.M. Laskowski RA, D.S. Moss, J.M. Thornton, PROCHECK: a program to check the stereochemical quality of protein structures, J. Appl. Cryst. 26 (1993) 283–291.
[45] G. Vriend, V. Eijsink, Prediction and analysis of structure, J. Comput. Aided Mol. Des. 7 (1993) 367–396.
[46] B. Rost, C. Sander, Prediction of protein secondary structure at better than 70% accuracy, J. Mol. Biol. 232 (1993) 584–599.
[47] B. Nagar, W.G. Bornmann, P. Pellicena, T. Schindler, D.R. Veach, W.T. Miller, B. Clarkson, J. Kuriyan, Crystal structures of the kinase domain of c-Abl in complex with the small molecule inhibitors PD173955 and imatinib (STI-571), Cancer Res. 62 (2002) 4236–4243.
[48] P.A. Keller, S.P. Leach, T.T. Luu, S.J. Titmuss, R. Griffith, Development of computational and graphical tools for analysis of movement and flexibility in large molecules, J. Mol. Graph Model. 18 (2000) 235–241, 299.
[49] D.R. Knighton, N.H. Xuong, S.S. Taylor, J.M. Sowadski, Crystallization studies of cAMP-dependent protein kinase. Cocrystals of the catalytic subunit with a 20 amino acid residue peptide inhibitor and MgATP diffract to 3.0 A resolution, J. Mol. Biol. 220 (1991) 217–220.
[50] W. Hemmer, M. McGlone, I. Tsigelny, S.S. Taylor, Role of the glycine triad in the ATP-binding site of cAMP-dependent protein kinase, J. Biol. Chem. 272 (1997) 16946–16954.
[51] S. Cox, E. Radzio-Andzelm, S.S. Taylor, Domain movements in protein kinases, Curr. Opin. Struct. Biol. 4 (1994) 893–901.
[52] S. Lev, D. Givol, Y. Yarden, Interkinase domain of kit contains the binding site for phosphatidylinositol 3′ kinase, Proc. Natl. Acad. Sci. U.S.A. 89 (1992) 678–682.
[53] K. Thommes, J. Lennartsson, M. Carlberg, L. Ronnstrand, Identification of Tyr-703 and Tyr-936 as the primary association sites for Grb2 and Grb7 in the c-Kit/stem cell factor receptor, Biochem. J. 341 (Pt. 1) (1999) 211–216.
[54] B.D. Grant, W. Hemmer, I. Tsigelny, J.A. Adams, S.S. Taylor, Kinetic analyses of mutations in the glycine-rich loop of cAMP-dependent protein kinase, Biochemistry 37 (1998) 7708–7715.
[55] M. Odawara, T. Kadowaki, R. Yamamoto, Y. Shibasaki, K. Tobe, D. Accili, C. Bevins, Y. Mikami, N. Matsuura, Y. Akanuma, et al., Human diabetes associated with a mutation in the tyrosine kinase domain of the insulin receptor, Science 245 (1989) 66–68.
[56] M.P. Cooke, R.M. Perlmutter, Expression of a novel form of the fyn proto-oncogene in hematopoietic cells, New Biol. 1 (1989) 66–74.
[57] J.H. Till, M. Becerra, A. Watty, Y. Lu, Y. Ma, T.A. Neubert, S.J. Burden, S.R. Hubbard, Crystal structure of the MuSK tyrosine kinase: insights into receptor autoregulation, Structure (Camb) 10 (2002) 1187–1196.
[58] M. Miller, K. Ginalski, B. Lesyng, N. Nakaigawa, L. Schmidt, B. Zbar, Structural basis of oncogenic activation caused by point mutations in the kinase domain of the MET proto-oncogene: modeling studies, Proteins 44 (2001) 32–43.
[59] C.D. Mol, K.B. Lim, V. Sridhar, H. Zou, E.Y. Chien, B.C. Sang, J. Nowakowski, D.B. Kassel, C.N. Cronin, D.E. McRee, Structure of a c-kit product complex reveals the basis for kinase transactivation, J. Biol. Chem. 278 (2003) 31461–31464.
[60] H. Serve, N.S. Yee, G. Stella, L. Sepp-Lorenzino, J.C. Tan, P. Besmer, Differential roles of PI3-kinase and Kit tyrosine 821 in Kit receptor-mediated proliferation, EMBO J. 14 (1995) 473–483.
[61] H. Kitayama, Y. Kanakura, T. Furitsu, T. Tsujimura, K. Oritani, H. Ikeda, H. Sugahara, H. Mitsui, Y. Kanayama, Y. Kitamura, et al., Constitutively activating mutations of c-kit receptor tyrosine kinase confer factor-independent growth and tumorigenicity of factor-dependent hematopoietic cell lines, Blood 85 (1995) 790–798.
[62] L.P. Lam, R.Y. Chow, S.A. Berger, A transforming mutation enhances the activity of the c-Kit soluble tyrosine kinase domain, Biochem. J. 338 (Pt. 1) (1999) 131–138.
[63] T. Tsujimura, K. Hashimoto, H. Kitayama, H. Ikeda, H. Sugahara, I. Matsumura, T. Kaisho, N. Terada, Y. Kitamura, Y. Kanakura, Activating mutation in the catalytic domain of c-kit elicits hematopoietic transformation by receptor self-association not at the ligand-induced dimerization site, Blood 93 (1999) 1319–1329.
[64] B.J. Longley Jr., D.D. Metcalfe, M. Tharp, X. Wang, L. Tyrrell, S.Z. Lu, D. Heitjan, Y. Ma, Activating and dominant inactivating c-KIT catalytic domain mutations in distinct clinical forms of human mastocytosis, Proc. Natl. Acad. Sci. U.S.A. 96 (1999) 1609–1614.
[65] T. Tsujimura, T. Furitsu, M. Morimoto, K. Isozaki, S. Nomura, Y. Matsuzawa, Y. Kitamura, Y. Kanakura, Ligand-independent activation of c-kit receptor tyrosine kinase in a murine mastocytoma cell line P-815 generated by a point mutation, Blood 83 (1994) 2619–2626.
[66] Y. Moriyama, T. Tsujimura, K. Hashimoto, M. Morimoto, H. Kitayama, Matsuzawa, Y. Kitamura, Y. Kanakura, Role of aspartic acid 814 in the function and expression of c-kit receptor tyrosine kinase, J. Biol. Chem. 271 (1996) 3347–3350.
[67] F.M. Abu-Duhier, A.C. Goodeve, G.A. Wilson, R.S. Care, I.R. Peake, J.T. Reilly, Identification of novel FLT-3 Asp835 mutations in adult acute myeloid leukaemia, Br. J. Haematol. 113 (2001) 983–988.
[68] A. Bardelli, P. Longati, D. Gramaglia, C. Basilico, L. Tamagnone, S. Giordano, D. Ballinari, P. Michieli, P.M. Comoglio, Uncoupling signal transducers from oncogenic MET mutants abrogates cell transformation and inhibits invasive growth, Proc. Natl. Acad. Sci. U.S.A. 95 (1998) 14379–14383.
[69] D. Fabbro, S. Ruetz, E. Buchdunger, S.W. Cowan-Jacob, G. Fendrich, J. Liebetanz, J. Mestan, T. O'Reilly, P. Traxler, B. Chaudhuri, H. Fretz, J. Zimmermann, T. Meyer, G. Caravatti, P. Furet, P.W. Manley, Protein kinases as targets for anticancer agents: from inhibitors to useful drugs, Pharmacol. Ther. 93 (2002) 79–98.
[70] D. Fabbro, D. Parkinson, A. Matter, Protein tyrosine kinase inhibitors: new treatment modalities? Curr. Opin. Pharmacol. 2 (2002) 374–381.
[71] A. Levitzki, Tyrosine kinases as targets for cancer therapy, Eur. J. Cancer 5 (Suppl. 38) (2002) S11–18.
[72] E.A. Sausville, Y. Elsayed, M. Monga, G. Kim, Signal transduction-directed cancer treatments, Annu. Rev. Pharmacol. Toxicol. 43 (2003) 199–231.
[73] J. Drevs, M. Medinger, C. Schmidt-Gersbach, R. Weber, C. Unger, Receptor tyrosine kinases: the main targets for new anticancer therapy, Curr. Drug Targets 4 (2003) 113–121.
[74] T. Schindler, W. Bornmann, P. Pellicena, W.T. Miller, B. Clarkson, J. Kuriyan, Structural mechanism for STI-571 inhibition of abelson tyrosine kinase, Science 289 (2000) 1938–1942.
[75] M. Azam, R.R. Latek, G.Q. Daley, Mechanisms of autoinhibition and STI-571/imatinib resistance revealed by mutagenesis of BCR-ABL, Cell 112 (2003) 831–843.
[76] R.A. Engh, D. Bossemeyer, Structural aspects of protein kinase control-role of conformational flexibility, Pharmacol. Ther. 93 (2002) 99–111.
[77] C. Merlot, D. Domine, C. Cleva, D.J. Church, Chemical substructures in drug discovery, Drug Discov. Today 8 (2003) 594–602.